Globally Significant Mass of Terrestrial Organic Carbon Efficiently Transported by Canyon-Flushing Turbidity Currents

Megan L. Baker[1], Sophie Hage[2], Peter J. Talling[1,3], Sanem Acikalin[4], Robert G. Hilton[5], Negar Haghipour[6,7], Sean C. Ruffell[3], Ed L. Pope[1], Ricardo Silva Jacinto[8], Michael A. Clare[9], Sefa Sahin[4]

[1]*Department of Geography, Durham University, Durham, DH1 3LE, UK*

[2]*University of Brest, CNRS, IFREMER, Geo-Ocean; 29280 Plouzané, France*

[3]*Department of Earth Sciences, Durham University, Durham, DH1 3LE, UK*

[4]*School of Civil Engineering and Geosciences, Newcastle University, Newcastle upon Tyne, NE1 7RU, UK*

[5]*Department of Earth Sciences, University of Oxford, Oxford, OX1 3AN, UK*

[6]*Geological Institute, ETH Zürich, 8092 Zürich, Switzerland*

[7]*Laboratory of Ion Beam Physics, ETH Zürich, 8093 Zurich, Switzerland*

[8]*Geo-OceanUnit, IFREMER Centre de Brest, 29280 Plouzané, France*

[9]*National Oceanography Centre, Southampton, SO14 3ZH, UK*

ABSTRACT

Burial of organic carbon in marine sediments is a long-term sink of atmospheric CO_2 and submarine turbidity currents are volumetrically the most important sediment transport process on Earth. Yet the processes, amounts, and efficiency of organic carbon transfer by turbidity currents through submarine canyons to the deep sea are poorly documented and understood. We present an organic carbon budget for the submarine Congo Canyon constrained with time-lapse bathymetry, sediment cores and flow monitoring, including the effects of two >1,000 km runout canyon-flushing turbidity currents. In one year, flows eroded an estimated 6.09 ± 2.70 Mt of previously-buried terrestrial organic carbon in the canyon, primarily from fine-grained and vegetation-rich muddy sand facies with high organic carbon contents (up to 11%). The age and composition of organic carbon in the Congo Canyon is comparable to that in the Congo River, indicating that transfer is efficient. Over the whole canyon-channel system, we extrapolate that 43 ± 15 Mt of organic carbon was eroded and transported to the deep (> 5 km) sea, equivalent to 22% of the annual global particulate organic carbon export from rivers to oceans, and 54-108% of the predicted annual terrestrial organic carbon burial in the oceans. Canyon-flushing turbidity currents carried a globally significant mass of terrestrial organic carbon down just one submarine canyon in a single year, indicating their importance for redistribution and delivery of organic carbon to the deep sea.

INTRODUCTION

Photosynthesis by plants removes CO_2 from the atmosphere and forms organic matter containing organic carbon (OC). A fraction of this terrestrial OC travels via rivers to the coast and is deposited in marine sediments (Blair and Aller, 2012). The burial of OC in marine sediments over geological timescales leads to a net drawdown of atmospheric CO_2, aiding regulation of the long-term climate (Berner, 1982; Hilton and West, 2020). It is increasingly recognized that OC can be efficiently transported and buried in the deep sea by turbidity currents travelling down active submarine canyons (e.g., Kao et al., 2014; Sparkes et al., 2015; Talling et al., 2024), with >9,500 canyons worldwide (Harris et al., 2014).

Many previous analyses of global OC burial in marine sediments overlooked the role of turbidity currents and submarine canyons (e.g., Berner, 1982; Burdige, 2005, 2007). Although many canyons are assumed inactive due to the current sea level high-stand, a number of canyons in a range of settings have remained active (Covault and Graham, 2010; Heijnen et al., 2022a). Studies indicate that the mass of OC transported through canyon-channels and buried in submarine fans (e.g., Bengal Fan, Congo Fan) can be significant (Galy et al., 2007; Rabouille et al., 2019).

Sediment and OC within canyons can undergo multiple cycles of erosion, transport and deposition via relatively small 'canyon-filling' turbidity currents, which runout in the canyon-channel. Occasionally, powerful and long runout 'canyon-flushing' turbidity currents erode and transport material to the depositional lobe (Heijnen et al., 2022b; Pope et al., 2022). Uncertainties in turbidity current recurrence intervals and runout distance are combined with limited measurements of quantity, age, and composition of OC in canyon-channel deposits. This has resulted in a knowledge gap on how turbidity currents move OC within canyons and, crucially, the potential for OC storage within this part of the global sedimentary system.

Here, for the first time, we combine time-lapse seafloor bathymetric maps, sediment cores, and direct flow-monitoring data to understand how OC is transferred and buried in the deep sea by turbidity currents. We present a well-constrained OC budget for the Congo Canyon, offshore West Africa, covering an exceptional one-year period when the canyon experienced two powerful (5-8 $m\ s^{-1}$) and long (>1,000 km) runout canyon-flushing flows (Talling et al., 2022). Our objectives are: (1) to show how OC is distributed within the Congo Canyon floor facies and derive an OC budget for the canyon; (2) upscale the OC canyon budget to quantify the mass of OC eroded from the Congo Canyon-Channel, and compare this value to global fluxes of terrestrial OC; (3) compare the Congo Canyon, River and Lobe OC signatures to produce a conceptual model for efficient transport of terrestrial OC through river-connected submarine canyons.

STUDY AREA AND METHODS

The Congo Canyon is directly connected to the Congo River, the second largest river in the world by discharge, and fifth largest for annual particulate OC export (Fig. 1; Babonneau et al., 2002; Coynel et al., 2005). In the deeply incised canyon, turbidity currents have been recorded for ~33% of the time during monitoring periods (Azpiroz-Zabala et al., 2017). At ~2,000 m water depth the canyon transitions to a less incised channel that continues downslope to the lobe at ~5,000 m water depth.

In September-October 2019, seven piston cores were collected from the canyon thalweg between 1577 m and 2173 m water depth. The cores were scanned with a Multi-Sensor Core Logger, split, and visually logged, with five sedimentary facies identified (Fig. 2). Individual beds could not be correlated between cores due to highly variable deposits. Seventy samples from different facies were analyzed for grain size. To determine the OC quantity, source (terrestrial or marine), and age, the same samples were analyzed for total organic carbon (TOC) content, carbon stable isotope composition ($\delta^{13}C$) and radiocarbon content (expressed as 'fraction modern', Fm, a measurement of the deviation of the $^{14}C/^{12}C$ ratio of a sample from "modern"; Supplemental Methods).

To record turbidity currents between October 2019 to May 2020, 11 acoustic Doppler current profiler (ADCP) moorings and 12 Ocean Bottom Seismographs (OBSs) were deployed along the Congo Canyon-Channel (Fig. 1; Talling et al., 2022; Supplemental Methods). A powerful turbidity current broke the moorings and two seafloor telecommunications cables on 14-16th January 2020, with the repaired cables broken again by a major flow on 8th March 2020.

To calculate the Congo Canyon OC budget, the net eroded sediment volume from the canyon floor was determined using the September-October 2019 and October 2020 multibeam surveys, collected with a Kongsberg EM122 echosounder (Fig. 1). The net eroded sediment volume was divided into the facies proportions averaged across the sediment cores and converted to sediment mass, using the average facies porosity ± 1 standard deviation to get sediment density (Table S1, S2). The OC mass eroded was calculated using the average TOC ± 1 standard deviation for each facies (Table S3). An OC budget for the full Congo Canyon-Channel was estimated using a facies porosity range and the TOC of Congo Channel sediments from Baudin et al. (2020), and a total eroded sediment volume of 2.68 km^3 (Talling et al., 2022; Supplemental Methods).

RESULTS

Sedimentary facies and organic carbon composition

The Congo Canyon thalweg cores contain five facies, which are now described along with their OC composition (Figs. 2 and 3; Table S3, S4): (1) **Clay** is homogenous or bioturbated and comprises 47% of the cores. The facies has a high TOC (reported as the mean, $TOC_{av,}$ ± 1 standard deviation) of 3.51 ± 0.60% and an OC age (reported as the mean Fm, Fm_{av} ± 1 standard deviation) of 0.94 ± 0.04. (2) **Silt** (18% of the cores) contains occasional laminations or normal grading to clay and may be homogeneous or bioturbated. This facies has OC Fm_{av} = 0.95 ± 0.02 and TOC_{av} = 2.60 ± 0.99%. (3) **Muddy sand** (22% of the cores) comprises mud with fine- to medium-grained sand, that may be ungraded or normally graded, and can contain clasts. This has a lower TOC_{av} = 1.81 ± 1.74%, and older OC (Fm_{av} = 0.91 ± 0.06) compared to clay or silt. (4) **Sand** comprises clean, fine- to medium-grained sand with rare clasts and is often ungraded or occasionally normally graded. Sand facies comprises 9% of the cores, with low TOC_{av} = 0.49 ± 0.26% and the oldest OC with Fm_{av} = 0.78 ± 0.06. (5) **Vegetation-rich muddy sand** contains concentrated, well-preserved mm- to cm-sized black wood and plant debris (Fig. 2C) within a fine-grained sand-mud matrix with no grading. This facies only makes up 4% of the cores but contains high TOC_{av} = 8.24 ±

2.24%, and the youngest OC, $Fm_{av} = 0.99 \pm 0.02$. Most of the facies $\delta^{13}C$ values are depleted (−28.5‰ to −26‰), indicating a terrestrial origin for the OC, consistent with Congo River sediment samples (Fig. 3B; Hemingway et al., 2017).

Turbidity currents in the canyon

The ADCP-moorings, cable breaks and OBS stations recorded 19 turbidity currents in the Congo Canyon-Channel over 8 months. The majority (17) of the flows terminated in the canyon (runout distance <190 km; 2 flows), or before reaching the deep-water channel (runout distance <791 km; 15 flows), with an average 3.7 m s^{-1} transit velocity (Fig. S1). However, two turbidity currents travelled >1,000 km and reached transit velocities of 5.7 and 7.6 m s^{-1}. These large, cable-breaking, flows were preconditioned by major river floods (with return intervals of 20-50 years), but occurred weeks to months after the flood peak, often during spring tides (Talling et al., 2022).

Sediment and organic carbon budget

The bathymetric difference map shows significant erosion occurred along the canyon thalweg over one year (Fig. 1C, D). The net eroded sediment volume along the 112 km-surveyed length of canyon is 0.32 km^3. This equates to 226 ± 36 Mt of sediment and 6.09 ± 2.70 Mt of terrestrial OC eroded over one year. The clay facies contributed the largest amount of eroded OC (3.13 ± 0.87 Mt), followed by silt (1.24 ± 0.60 Mt), muddy sand (0.91 ± 0.88 Mt), vegetation-rich muddy sand (0.66 ± 0.25 Mt) and sand (0.15 ± 0.09 Mt; Fig. 3D).

DISCUSSION

How is organic carbon distributed within the Congo Canyon thalweg?

The Congo Canyon thalweg contains varied sedimentary deposits, with a strong link between facies type and TOC. The $\delta^{13}C$ values indicate that the OC has a terrestrial source. Overall, 6.09 ± 2.70 Mt of OC was eroded in the Congo Canyon over one year (Fig. 3). The cores are dominated by high TOC, fine-grained facies (69% clay and silt) which held 72% of the canyon OC budget (Fig 3C, D), showing that the canyon of this mud-rich system is primarily fine-grained. Clay and silt are associated with high TOC values as minerals in these sediments form chemical bonds with OC, preventing oxidation (Hemingway et al., 2019). The age of the clay and silt OC (Fm_{av} of 0.94 ± 0.04 and 0.95 ± 0.02) likely corresponds to a mixture of young terrestrial biospheric OC and old terrestrial biospheric OC from degraded organic matter in the Congo Basin, as indicated by Congo River OC Fm of 0.89 ± 0.07 (Hemingway et al., 2017).

The Congo Canyon cores contain only a modest amount of sand (9%) and muddy sand (18%). These sand-rich facies contained low TOC, and thus provided only 17% of the OC in the budget (Fig 3D). The sand facies contained the oldest OC in the canyon (Fm_{av} = 0.78 ± 0.06). This suggests large contributions to the bulk Fm measurements from old terrestrial biospheric OC or petrogenic OC (^{14}C-free OC from eroded rocks), as seen in coarse-grained deposits in other turbidite systems (e.g., Hage et al., 2020).

The vegetation-rich muddy sand facies made up only 4% of the total facies yet contributed 11% of the canyon OC budget due to a high TOC_{av} of 8.24 ± 2.24% (Fig. 3). Prior work in turbidite systems also concluded that sandy facies can contribute to OC burial in marine sediments due to plant debris (Lee et al., 2019; Hage et al., 2020). However, these studies observed plant debris in cleaner-sand turbidite units (i.e., T_B and T_D of the Bouma sequence), rather than the muddy-sand matrix that contained plant debris in the Congo Canyon. This suggests different hydrodynamic sorting of plant debris by mud-rich turbidity currents compared to sandy flows. The vegetation-rich muddy sand had a Fm_{av} = 0.99 ± 0.02, indicating the dominance of young terrestrial biospheric OC derived recently from the atmosphere (within the last ~100 years). Burial of this fresh material in marine sediments represents a relatively rapid removal of CO_2 from the atmosphere (Lee et al., 2019).

Comparison of organic carbon eroded along the Congo Canyon-Channel to global fluxes

The >1,000 km runout flows eroded 2.68 km^3 of seabed sediment along the Congo Canyon-Channel (Talling et al., 2022). Facies and TOC trends down the Congo Channel are poorly constrained. Cores suggest there is a transition from the diverse, TOC-rich canyon sediments to sandy channel sediments with an estimated TOC of 2.0 ± 0.1%. (Baudin et al., 2010, 2017, 2020). Using this TOC value for the remaining 2.36 km^3 of eroded sediment, we estimate that 43 ± 15 Mt of terrestrial OC was eroded along the Congo Canyon-Channel in one year by two canyon-flushing turbidity currents (Supplemental Methods). This is a globally-significant mass of eroded OC, equivalent to 22% of annual global particulate OC export from all rivers to the oceans (200 Mt/year; Galy et al., 2015) and 54-108% of the annual terrestrial OC predicted to be buried in the global ocean (40-80 Mt/yr; Hilton and West, 2020). While the return interval of canyon-flushing flows and the annual rate of OC transfer by turbidity currents cannot yet be assessed, this study shows that the mass of terrestrial OC transferred to the deep sea by turbidity currents can contribute to global OC fluxes.

Efficient transport of terrestrial organic carbon through river-connected submarine canyons

Direct monitoring recorded multiple low-velocity ‘canyon-filling’ turbidity currents terminating in the Congo Canyon-Channel. Two faster, >1,000 km runout, strongly erosive ‘canyon-flushing’ events were also recorded (Fig. S1). This is consistent with magnitude-frequency-runout studies of shallow-water turbidity currents (Heerema et al., 2020; Heijnen et al., 2022b). These flow observations are combined with OC signature data in the Congo River, Canyon, and Lobe to inform our OC transport model (Fig. 4).

The canyon-filling flows rapidly bury sediment and OC in the upper canyon-channel, helping to protect OC from degradation, and producing high TOC deposits (Fig. 4B; Hedges and Keil, 1995). Frequent canyon-filling flows may erode and rework the sediment and OC, exposing the OC to oxygenating conditions. However, despite such reworking, the age and origin of terrestrial OC in the Congo Canyon (Fm = 0.92 ± 0.08; $\delta^{13}C$ = -26.91 ± 0.84) is similar to that of terrestrial OC in the Congo River (Fm = 0.89 ± 0.07; $\delta^{13}C$ = -26.44 ± 0.77; Hemingway et al., 2017). This suggests highly efficient OC transport through this part of the system on contemporary timescales.

The OC deposited in the upper canyon-channel is temporarily stored for ~10s of years, before canyon-flushing flows, triggered by river floods with recurrence intervals of 20-50 years (Talling et al., 2022), erode the material and quickly transport it to the deep sea, along with relatively fresh OC from the Congo River floods (Fig. 4C). Flushed material is rapidly deposited on the lobe, protecting OC from degradation, and sequestering OC for long timescales (Galy et al., 2007). The Congo Lobe OC age has been measured as Fm = 0.89 and Fm = 0.80 (Savoye et al., 2009), which is similar to Congo Canyon and River Fm-values, supporting this model for efficient OC transport from river-mouth to lobe. Thus, canyon-flushing turbidity currents can efficiently transport globally significant amounts of terrestrial OC to the deep sea, indicating their importance for organic carbon budgets.

ACKNOWLEDGMENTS

We thank the officers and crew on RRS James Cook. Research was funded by UK NERC grants NE/R001952/1, NE/V004387/1, NE/R015953/1 and NE/S010068/1, Leverhulme Trust Early Career Fellowships ECF-2018-267 and ECF-2021-566, and Newcastle University internal funding. RGH was funded by the Visiting Professor scheme at the Geological Institute, ETH

Zürich. SH was funded by the European Union's Horizon 2020 research and innovation programme under the Marie Sklodowska-Curie grant No 899546.

REFERENCES CITED

Azpiroz-Zabala, M., Cartigny, M.J.B., Talling, P.J., Parsons, D.R., Sumner, E.J., Clare, M.A., Simmons, S.M., Cooper, C., and Pope, E.L., 2017, Newly recognized turbidity current structure can explain prolonged flushing of submarine canyons: Science Advances, v. 3, doi:10.1126/sciadv.1700200.

Babonneau, N., Savoye, B., Cremer, M., and Klein, B., 2002, Morphology and architecture of the present canyon and channel system of the Zaire deep-sea fan: Marine and Petroleum Geology, v. 19, p. 445–467, doi:10.1016/S0264-8172(02)00009-0.

Baudin, F., Disnar, J.R., Martinez, P., and Dennielou, B., 2010, Distribution of the organic matter in the channel-levees systems of the Congo mud-rich deep-sea fan (West Africa). Implication for deep offshore petroleum source rocks and global carbon cycle: Marine and Petroleum Geology, v. 27, p. 995–1010, doi:10.1016/j.marpetgeo.2010.02.006.

Baudin, F., Martinez, P., Dennielou, B., Charlier, K., Marsset, T., Droz, L., and Rabouille, C., 2017, Organic carbon accumulation in modern sediments of the Angola basin influenced by the Congo deep-sea fan: Deep-Sea Research Part II: Topical Studies in Oceanography, v. 142, p. 64–74, doi:10.1016/j.dsr2.2017.01.009.

Baudin, F., Rabouille, C., and Dennielou, B., 2020, Routing of terrestrial organic matter from the Congo River to the ultimate sink in the abyss: a mass balance approach: Geologica Belgica, v. 23, p. 41–52, doi:10.20341/gb.2020.004.

Berner, R.A., 1982, Burial of organic carbon and pyrite sulfur in the modern ocean: American

Journal of Science, v. 282, p. 451–473.

Blair, N.E., and Aller, R.C., 2012, The Fate of Terrestrial Organic Carbon in the Marine Environment: Annual Review of Marine Science, v. 4, p. 401–423, doi:10.1146/annurev-marine-120709-142717.

Burdige, D.J., 2005, Burial of terrestrial organic matter in marine sediments: A re-assessment: Global Biogeochemical Cycles, v. 19, p. 1–7, doi:10.1029/2004GB002368.

Burdige, D.J., 2007, Preservation of organic matter in marine sediments: Controls, mechanisms, and an imbalance in sediment organic carbon budgets? Chemical Reviews, v. 107, p. 467–485, doi:10.1021/cr050347q.

Covault, J.A., and Graham, S.A., 2010, Submarine fans at all sea-level stands: Tectono-morphologic and climatic controls on terrigenous sediment delivery to the deep sea: Geology, v. 38, p. 939–942, doi:10.1130/G31081.1.

Coynel, A., Seyler, P., Etcheber, H., Meybeck, M., and Orange, D., 2005, Spatial and seasonal dynamics of total suspended sediment and organic carbon species in the Congo River: Global Biogeochemical Cycles, v. 19, p. 1–17, doi:10.1029/2004GB002335.

Galy, V., France-Lanord, C., Beyssac, O., Faure, P., Kudrass, H., and Palhol, F., 2007, Efficient organic carbon burial in the Bengal fan sustained by the Himalayan erosional system: Nature, v. 450, p. 407–410, doi:10.1038/nature06273.

Galy, V., Peucker-Ehrenbrink, B., and Eglinton, T., 2015, Global carbon export from the terrestrial biosphere controlled by erosion: Nature, v. 521, p. 204–207, doi:10.1038/nature14400.

Hage, S. et al., 2020, Efficient preservation of young terrestrial organic carbon in sandy turbidity-current deposits: Geology, v. 48, p. 882–887, doi:10.1130/G47320.1.

Harris, P.T., Macmillan-Lawler, M., Rupp, J., and Baker, E.K., 2014, Geomorphology of the oceans: Marine Geology, v. 352, p. 4–24, doi:10.1016/j.margeo.2014.01.011.

Hedges, J.I., and Keil, R.G., 1995, Sedimentary organic matter preservation: an assessment and speculative synthesis: Marine Chemistry, v. 49, p. 81–115, doi:10.1016/0304-4203(95)00008-F.

Heerema, C.J. et al., 2020, What determines the downstream evolution of turbidity currents? Earth and Planetary Science Letters, v. 532, p. 116023, doi:10.1016/j.epsl.2019.116023.

Heijnen, M.S. et al., 2022a, Challenging the highstand-dormant paradigm for land-detached submarine canyons: Nature Communications, v. 13, p. 1–11, doi:10.1038/s41467-022-31114-9.

Heijnen, M.S. et al., 2022b, Fill, flush or shuffle: How is sediment carried through submarine channels to build lobes? Earth and Planetary Science Letters, v. 584, p. 117481, doi:10.1016/j.epsl.2022.117481.

Hemingway, J.D., Rothman, D.H., Grant, K.E., Rosengard, S.Z., Eglinton, T.I., Derry, L.A., and Galy, V. V., 2019, Mineral protection regulates long-term global preservation of natural organic carbon: Nature, v. 570, p. 228–231, doi:10.1038/s41586-019-1280-6.

Hemingway, J.D., Schefuß, E., Spencer, R.G.M., Dinga, B.J., Eglinton, T.I., McIntyre, C., and Galy, V. V., 2017, Hydrologic controls on seasonal and inter-annual variability of Congo River particulate organic matter source and reservoir age: Chemical Geology, v. 466, p. 454–465, doi:10.1016/j.chemgeo.2017.06.034.

Hilton, R.G., and West, A.J., 2020, Mountains, erosion and the carbon cycle: Nature Reviews Earth and Environment, v. 1, p. 284–299, doi:10.1038/s43017-020-0058-6.

Kao, S.J. et al., 2014, Preservation of terrestrial organic carbon in marine sediments offshore

Taiwan: Mountain building and atmospheric carbon dioxide sequestration: Earth Surface Dynamics, v. 2, p. 127–139, doi:10.5194/esurf-2-127-2014.

Lee, H., Galy, V., Feng, X., Ponton, C., Galy, A., France-Lanord, C., and Feakins, S.J., 2019, Sustained wood burial in the Bengal Fan over the last 19 My: Proceedings of the National Academy of Sciences of the United States of America, v. 116, p. 22518–22525, doi:10.1073/pnas.1913714116.

Pope, E.L. et al., 2022, First source-to-sink monitoring shows dense head controls sediment flux and runout in turbidity currents: Science Advances, v. 8, doi:10.1126/sciadv.abj3220.

Rabouille, C. et al., 2019, Carbon and silica megasink in deep-sea sediments of the Congo terminal lobes: Quaternary Science Reviews, v. 222, doi:10.1016/j.quascirev.2019.07.036.

Savoye, B., Babonneau, N., Dennielou, B., and Bez, M., 2009, Geological overview of the Angola-Congo margin, the Congo deep-sea fan and its submarine valleys: Deep-Sea Research Part II: Topical Studies in Oceanography, v. 56, p. 2169–2182, doi:10.1016/j.dsr2.2009.04.001.

Sparkes, R.B., Lin, I.T., Hovius, N., Galy, A., Liu, J.T., Xu, X., and Yang, R., 2015, Redistribution of multi-phase particulate organic carbon in a marine shelf and canyon system during an exceptional river flood: Effects of Typhoon Morakot on the Gaoping River-Canyon system: Marine Geology, v. 363, p. 191–201, doi:10.1016/j.margeo.2015.02.013.

Talling, P.J. et al., 2022, Longest sediment flows yet measured show how major rivers connect efficiently to deep sea: Nature Communications, v. 13, p. 1–15, doi:10.1038/s41467-022-31689-3.

Talling, P.J., Hage, S., Baker, M.L., Bianchi, T.S., Hilton, R.G., and Maier, K.L., 2024, The

Global Turbidity Current Pump and Its Implications for Organic Carbon Cycling: Annual Review of Marine Science, v. 16, p. 1–29, doi:10.1146/annurev-marine-032223-103626.

FIGURE CAPTIONS

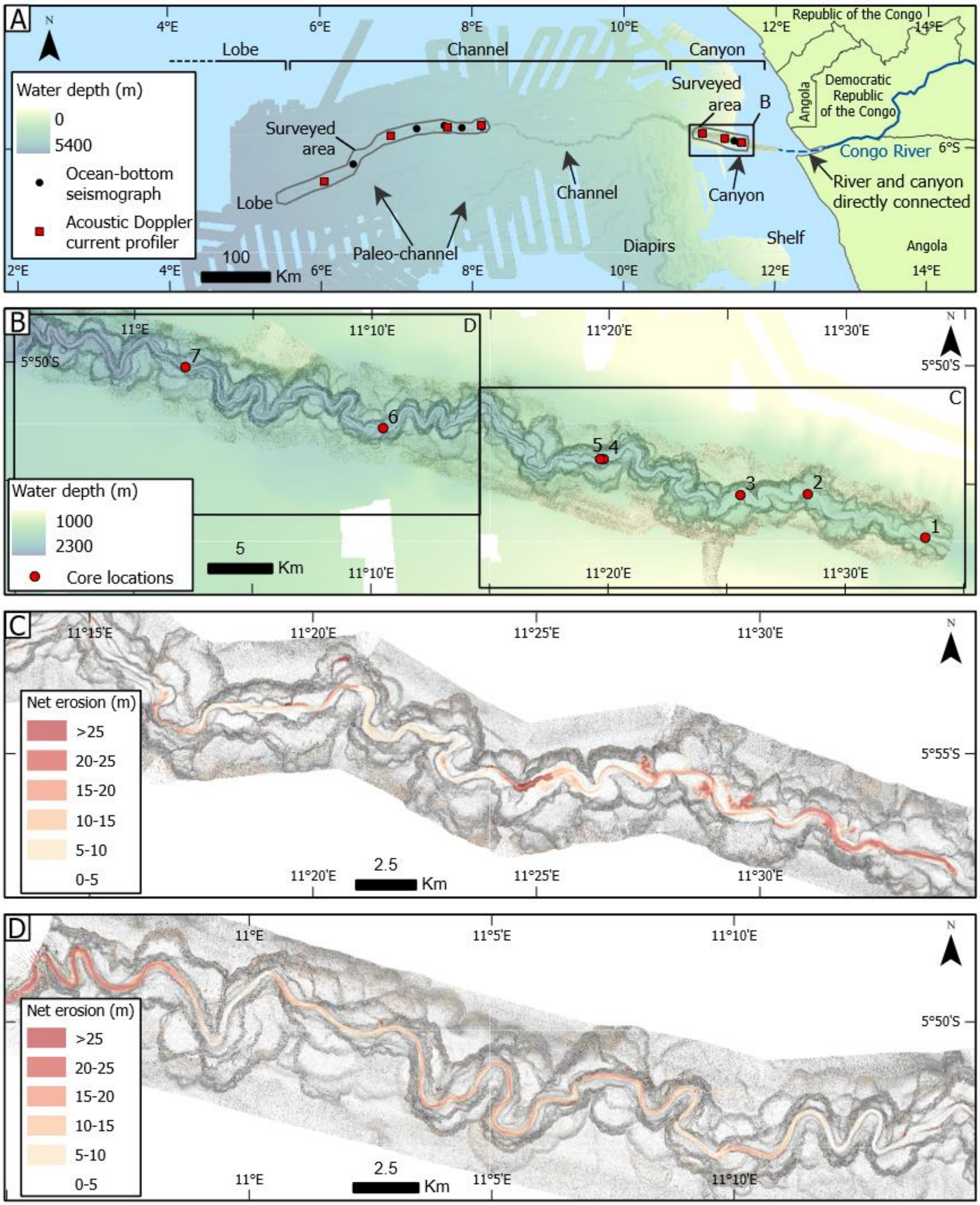

Figure 1. Study site. A) Bathymetric map of the Congo Submarine Fan (offshore West Africa) and instruments deployed to record turbidity currents. B) 2019 Congo Canyon bathymetry and

sediment core sites. C) and D) October 2019 – October 2020 elevation difference map showing canyon thalweg net erosion.

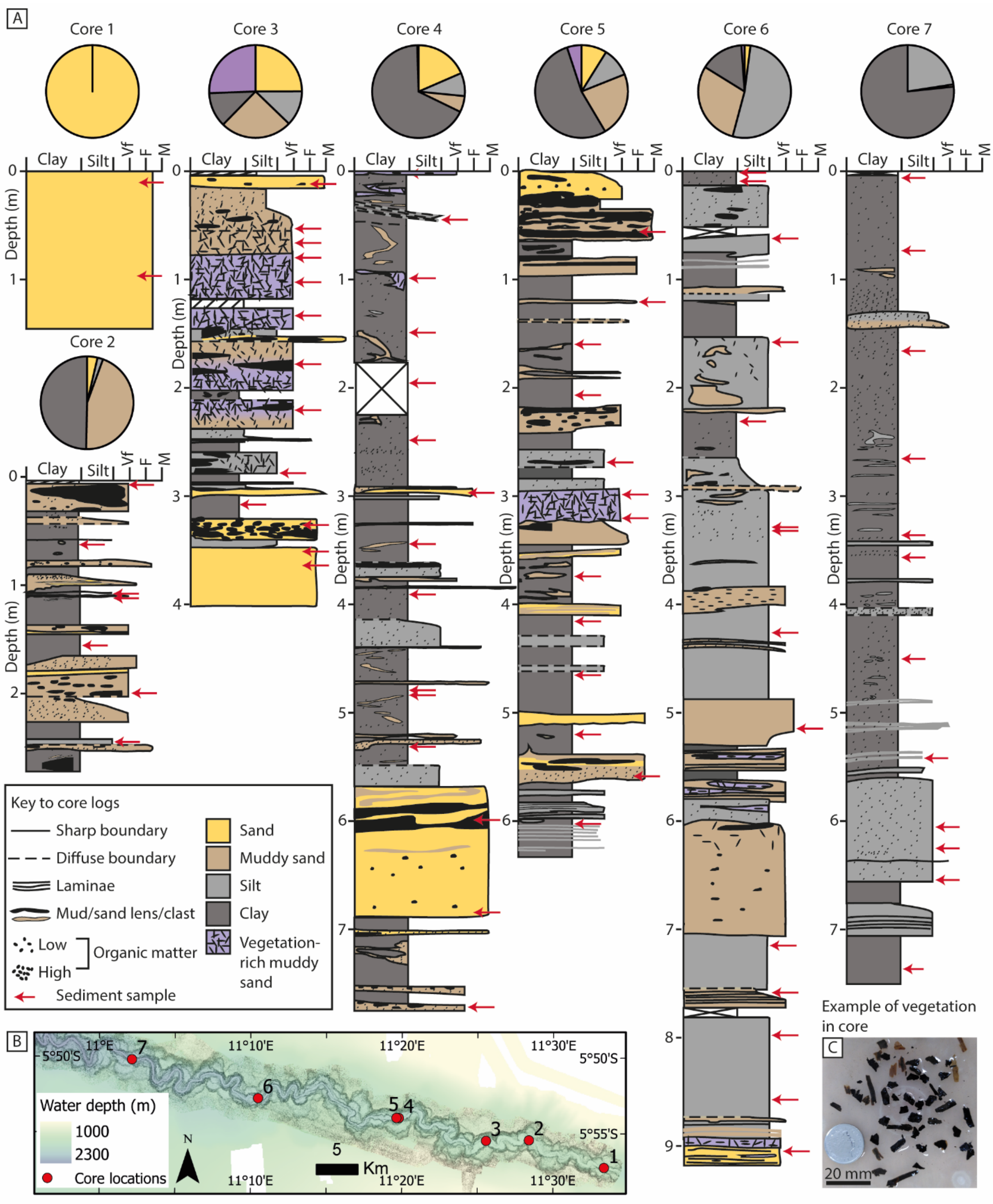

Figure 2. Congo Canyon thalweg cores collected October 2019. A) Core logs show the diverse range of facies eroded by 2020 canyon-flushing turbidity currents. B) Map of core locations. C) Photo of mm-size plant debris in the cores.

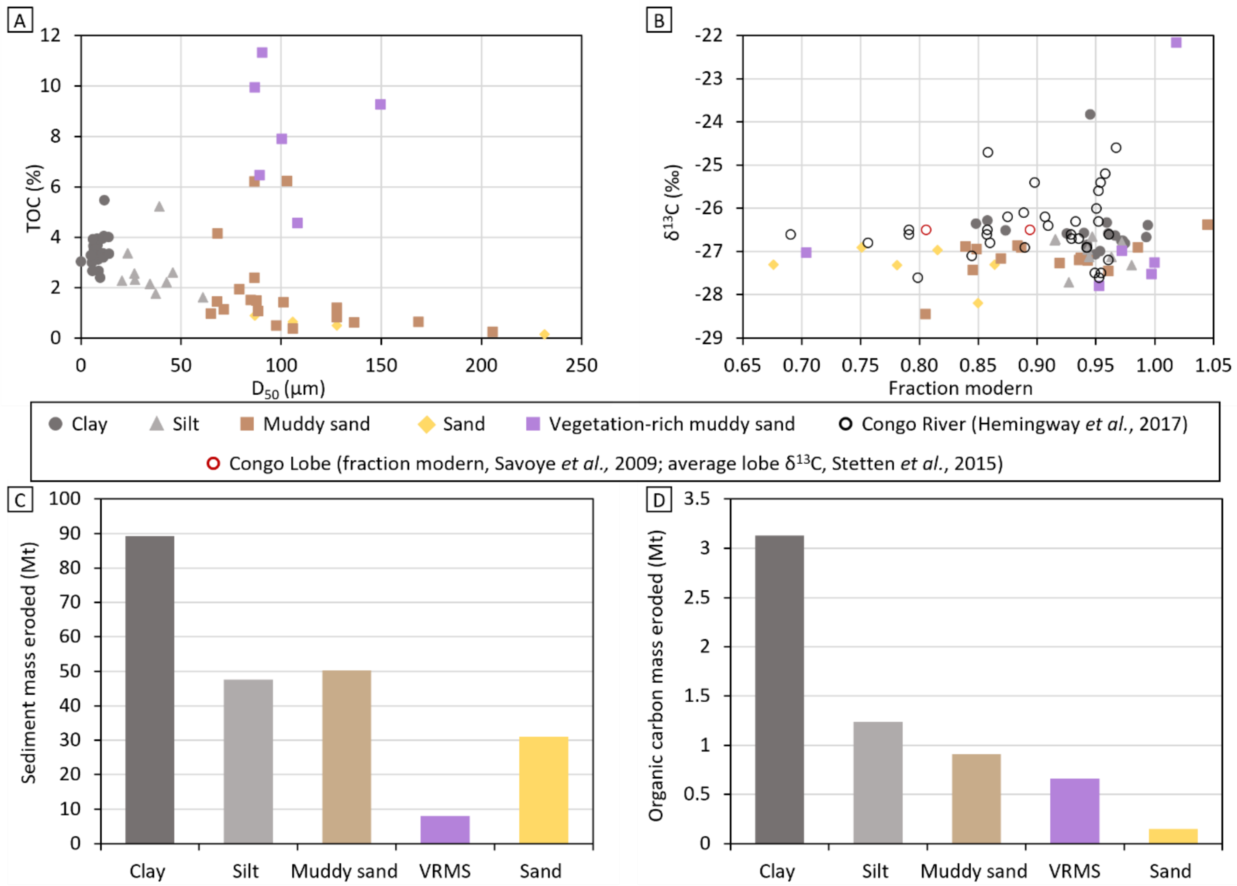

Figure 3. Congo Canyon organic carbon data and budget by facies. A) Total organic carbon (TOC) content against median grain size (D50). B) Carbon stable isotope ratios ($\delta^{13}C$) versus radiocarbon age (fraction modern), with published data from Congo River and Lobe. C) Sediment and D) organic carbon mass eroded from the canyon in one year.

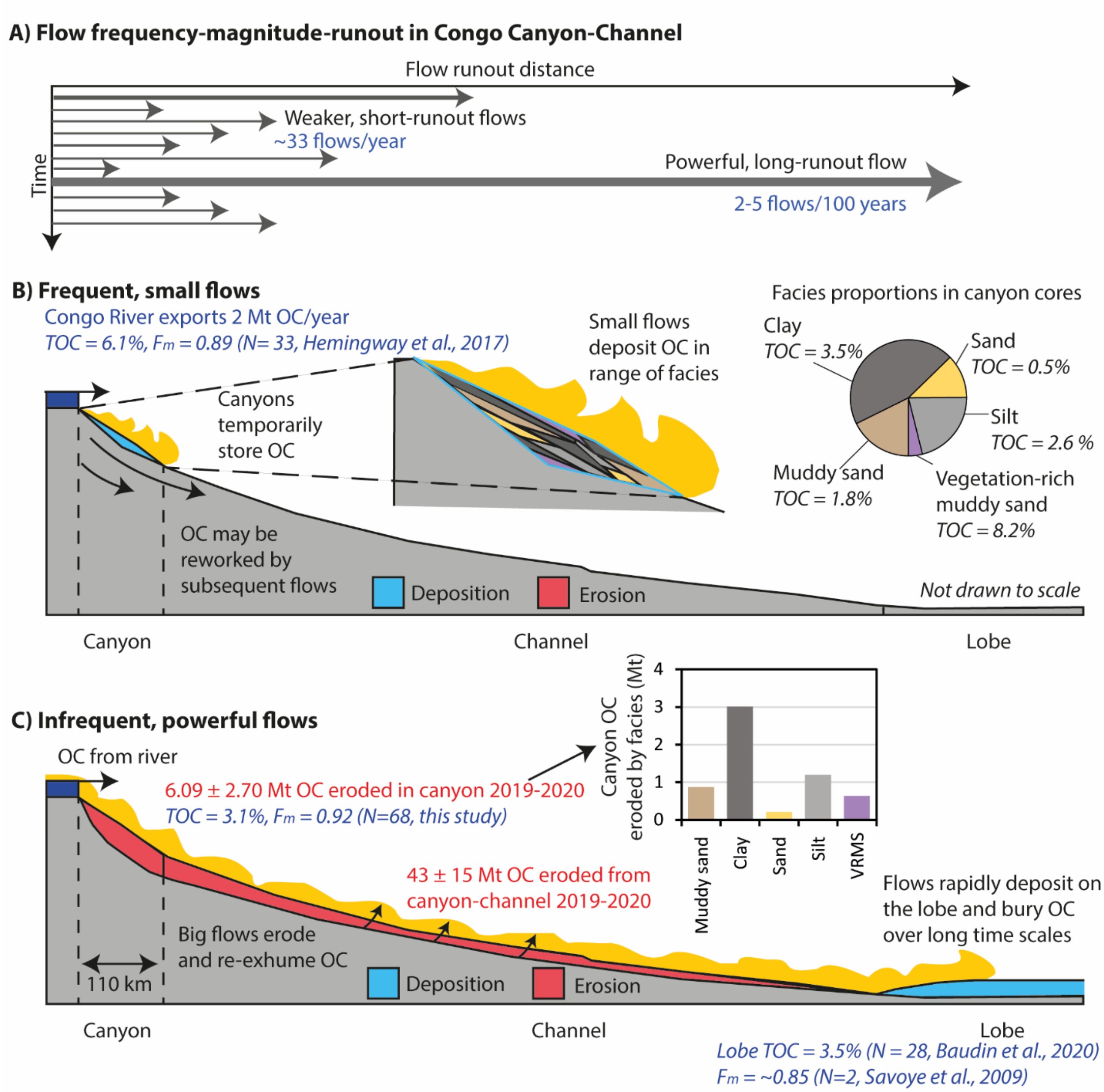

Figure 4. Efficient transport of terrestrial organic carbon (OC) through active submarine canyons connected to rivers. A) Congo Canyon-Channel turbidity currents are mainly ‘canyon-filling’ flows with occasional ‘canyon-flushing’ flows. B) Canyon-filling flows deposit sediment and organic carbon in a range of facies. C) Canyon-flushing flows erode and transport sediment and organic carbon to the lobe for long-term burial. VRMS = vegetation-rich muddy sand.

[1]Supplemental Material. Supplemental Methods (Deployment and specification of monitoring equipment, turbidity current identification, time-lapse seafloor surveys and analysis of sediment samples). Tables S1–S5 and Figure S1. Please visit https://doi.org/10.1130/XXXX to access the supplemental material, and contact editing@geosociety.org with any questions.

SUPPLEMENTAL METHODS

Field deployment of ADCP moorings and OBSs

Eleven moorings with acoustic-Doppler current profilers (ADCPs) and twelve Ocean-Bottom Seismographs (OBSs) were deployed along the Submarine Congo Canyon-Channel between 9th September 2019 to 2nd October 2019, divided into canyon and channel sub-arrays (Fig. 1). The ADCPs were on a fixed mooring anchored within the canyon-channel, suspended 44-250 m above the canyon floor. In contrast, the OBS were deployed ~700-2900 m outside the canyon-channel, on flat canyon terraces or on overbank areas. The location of each OBS is based on the ship's position when the instrument was deployed, whilst the location of each ADCP mooring was confirmed to within +/- ~15 m by ultra-short baseline acoustic positioning. Three ADCP moorings surfaced in October 2019, while the remaining eight were broken by the powerful, >1,000 km runout 14-16th January 2020 turbidity current event, which also broke the SAT-3 (South Atlantic 3) and WACS (West Africa Cable System) cables. A second >1,000 km runout flow on 8th March 2020 broke the repaired SAT-3 cable. The OBSs were not damaged by the >1,000 km runout flows and recorded ~9-10 months of data, depending on battery life. Nine of eleven ADCP and ten of twelve OBS instruments were recovered. Figure 1 shows the locations of the ADCPs and OBSs used in the analysis.

OBS and ADCP instrument specifications

Eight of the nine recovered OBS stations consisted of three channel Sercel L28-LB geophones and a Hi-Tech HTI-90U hydrophone. The most distal seismic station (OBS9), located 1071 km offshore, contained a three channel Owen (4.5Hz) Geophone and a Hi-Tech HTI-04 hydrophone. The geophone data were analysed for turbidity current activity, which recorded the ground vibrations generated by passing turbidity current events, with all geophones having a sampling frequency of 1 kHz.

The downward pointing ADCPs deployed were a mixture of 75, 300, and 600 kHz ADCPs, which recorded a profile of water column velocity every 11 or 45 seconds, depending on the ADCP set-up (Talling et al., 2022; their Supplementary Table 2).

Identifying turbidity current events in ADCP and OBS data and calculating flow transit velocities

Turbidity currents were identified in the ADCP data by an abrupt increase in near-bed velocities above ambient values of ~0.3 m/s, and the start manually picked. The start of a turbidity current event at each OBS was manually picked from the exponential curve on vertical component of the seismic data, at the point that the signal increased above background due to a passing turbidity current.

The transit speed of the turbidity currents was calculated by dividing the distance between ADCP or OBS stations (measured along the sinuous canyon thalweg) with the difference in arrival times. The distance the flows travelled (runout distance) was defined as the location of the most distal station that a tracked flow signal was recorded at.

The timing of submarine telecommunication cables breaks were also used to define turbidity current arrival times and transit velocities. Here we assume that the time of the fault equals the time of the arrival of the turbidity current. Cable breaks were recorded to the nearest minute.

Time-lapse seafloor surveys and net eroded sediment volumes

Bathymetric data of the Congo Canyon and Channel was collected via swath multibeam surveys collected in September–October 2019 and October 2020 using a Kongsberg EM122 (1° x 1°) system operating at 12 kHz on the RRS James Cook (Fig. 1A). The beam swath width was set to the narrowest setting (45° from the nadir) to try and generate the highest resolution data possible.

The data were processed in CARIS HIPS and SIPS and corrected for the ship's motion and for differences in sound velocity in the water column (using data from a sound-velocity profiler). The data was gridded with horizontal grid cell dimension of 5 m (canyon survey) or 15 m (channel survey).

Erosion or deposition of sediment between the two surveys was determined by producing a bathymetric difference map in ArcGIS, where the September-October 2020 bathymetric data was subtracted from September–October 2019 bathymetric data (Fig. 1C, D). The bathymetric difference map shows the net change in seafloor elevation over the one-year period between the two bathymetry surveys. To derive the volume of net eroded sediment, the change in elevation for each grid cell within the canyon thalweg and channel floor were multiplied by grid cell areas. Volumes of net erosion did not include areas outside the canyon or channel.

The net eroded volume calculations assumes that measurement errors are symmetrically distributed about a zero value, and thus cancel out over the survey areas. This was confirmed with measurements of differences in seabed elevation on the bathymetric difference map for areas where it was assumed no significant change occurred for both the canyon and channel. For these areas, the mean difference in seabed elevation was generally found to be close to zero with the difference values equally distributed around the mean when plotted as a histogram (Talling et al. 2020; supplementary figures 7 and 8). This method thus returns a 'best guess' for volume of seabed change.

To calculate the organic carbon mass eroded along the length of canyon and channel, we used the total net eroded sediment volume (2.68 km^3) determined by Talling et al. (2022). For this calculation, Talling et al. (2022) used both the canyon and channel time-lapse surveys (Fig 1). These two surveys covered 40% (477 km of 1179 km) of entire length of the Congo Canyon-Channel, as measured along its sinuous axis. Talling et al. (2022) assumed similar rates of erosion in the intervening section of channel that was not surveyed, to calculate the total net eroded volume of sediment along the whole canyon-channel system.

Grain size and geochemical analysis of sediment samples

Grain-size analysis of the sediment samples was conducted on the Beckman Coulter LS 13 320 Laser Diffraction Particle Size Analyser at the Department of Geography, Durham University. 20 mL of 20% hydrogen peroxide was added to ~0.5 g of sediment sample to remove organics before the sample was centrifuged to remove the supernatant. Samples were then mixed with 20 mL of deionized water and 2 mL of sodium hexametaphosphate solution to limit flocculation. Samples were run through the analyser three times; the runs were compared and if similar then the results were averaged.

The five core facies were identified as the sediment cores were visually logged based on visual characteristics and the feel of the material when rubbed between fingers. Clay bed facies were determined based on only smooth material felt between fingers, whilst silt contained a slight grittiness felt between fingers but with no grains visible using a hand-lens. The sand facies all had grains felt between fingers and visible with a hand lens, allowing the grain size to be determined. Muddy sand contained dark smooth mud in addition to the sand grains, whilst the sand facies was clean. Vegetation-rich muddy sand contained concentrated, well-preserved mm- to cm-sized black wood and plant debris, along with sand grains and a muddy matrix.

The carbon stable isotope composition ($\delta^{13}C$) of organic carbon (OC) is used to differentiate between marine and terrestrial organic matter, based on the assumption that marine organic matter is more depleted in ^{13}C compared to terrestrial organic matter (Burdige, 2005). Radiocarbon measurements were employed to determine the age of the OC and is expressed as 'fraction modern' (Fm). Fm is a measurement of the deviation of the $^{14}C/^{12}C$ ratio of a sample from "modern" (defined as 95% of the radiocarbon concentration in AD 1950). The Fm measurements are a bulk measurement of the sample, and thus the values can represent organic material of many ages and sources. Bulk OC Fm values can contain contributions from young terrestrial biospheric carbon produced by photosynthesis (Fm = ~1.0), old terrestrial biospheric carbon produced by degraded soil, and ancient (petrogenic) carbon from erosion of rocks which is ^{14}C free (Fm = 0) (Leithold et al., 2016; Hage et al., 2020). Future work could use additional techniques such as ramped pyrolysis–oxidation (RPO) to distinguish OC components.

Each sediment sample was measured for total organic carbon content (TOC), carbon stable isotope composition ($\delta^{13}C$) and radiocarbon content (expressed as 'fraction modern', Fm) at the Laboratory of Ion Beam Physics at ETH Zurich. About 60 mg of sediment was replaced in Ag capsules and treated with HCL 37% (65°C, 72 hours) to remove inorganic carbon. After neutralization with NaOH (65°C, 72 hours) samples were wrapped in tin boats. The TOC, radiocarbon and $\delta^{13}C$ composition of bulk OC were measured on an Elemental Analyzer-Isotope Ratio Mass Spectrometer (EA-IRMS, Elementar vario MICRO cube—Isoprime PresION) coupled to a Mini Carbon Dating System (MICADAS) Accelerator Mass Spectrometer. Based on peptone (Sigma) and atropine (Santis) standards, accuracy of TOC and $\delta^{13}C$, corresponded to values better than 0.03% and 0.1‰. Radiocarbon isotopic data were reduced using BATS software (Wacker et al., 2010) and reported radiocarbon data are expressed as F14 C (Fm) values (Reimer et al., 2004).

Published radiocarbon data from the Congo River from Hemingway et al. (2017), reported in Δ14C per-mille (‰) notation, was converted to Fm using:

$$F_m = \frac{\Delta 14C + 1000e^{-\frac{-(y-1950)}{8267}}}{1000}$$

Where *y* is the year of data collection (Torn et al., 2009). The radiocarbon data from the Congo Lobe in Savoye et al. (2009) were converted from radiocarbon years (conventional 14C age) to Fm using the following equation:

$$14C\ age = -8033Ln(F_m)$$

Organic carbon budget calculations

For the Congo Canyon organic carbon budget calculation, the total eroded sediment volume for the canyon floor (determined from the bathymetric difference map) needed to be converted to eroded dry sediment mass, via the sediment density (Tables S1 to S3). For this, the total eroded sediment volume was divided into the facies proportions averaged across the seven sediment cores (Table S1). This method assumes that the facies proportions, and associated facies sediment density within the cores, can be scaled up to represent the whole canyon floor. However, this is considered more precise than methods which assume blanket sediment density properties to convert from volume to mass.

To calculate the sediment density of each facies type, the porosity (ϕ) of the different facies was first derived from the gamma-ray wet density (ρ_w) values measured every 0.01 m from the Multi-Sensor Core Logger (GeoTek MSCL-S) via:

$$\phi = -\frac{(\rho_w - \rho_d)}{\rho_d - \rho_{sw}}$$

where ρ_{sw} is the density of seawater at 1.025 kg/m^3 and ρ_d is the sediment grain density of quartz at 2.6 kg/m^3. The average porosity for each facies in the sediment cores was averaged across six of the sediment cores and the standard deviation calculated, with core 1 discounted as the sediment had been remobilised (Table S2). The average facies porosity values ± standard deviation were converted into dry sediment density (ρ) using:

$$\rho = (1 - \phi) * \rho_d * 1000$$

From the dry sediment density, the facies mass eroded in Mt (Table S3) was calculated via:

$$M_f = (V * F) * \rho$$

where V is the total eroded volume in the canyon 0.32 km^3 and F is the facies proportion. The organic carbon mass eroded was then calculated using the average TOC (%) value ± standard deviation for each facies type (Table S3).

To calculate the organic carbon mass eroded along the length of canyon and channel, the total net eroded sediment volume along the whole canyon-channel determined by Talling et al. (2022) was used (2.68 km^3). First, the volume of sediment eroded from the canyon (0.32 km^3), for which the OC mass eroded was already well constrained, was subtracted from the total net eroded sediment volume. The remaining volume was converted to sediment and organic carbon mass using the estimated porosity and TOC values for the Congo Channel from Baudin et al. (2020). Baudin et al. (2020) suggest a porosity of 0.70% for sediment in the channel, to calculate the sediment mass we used a porosity range of 0.60% to 0.80%, based on global data for the upper 50 m of sediment (Kominz et al., 2011). A TOC value of 2.0 ± 0.1 % is used from Baudin et al. (2020) to convert from sediment to organic carbon mass.

REFERENCES

Baudin, F., Rabouille, C., and Dennielou, B., 2020, Routing of terrestrial organic matter from the Congo River to the ultimate sink in the abyss: a mass balance approach: Geologica Belgica, v. 23, p. 41–52, doi:10.20341/gb.2020.004.

Burdige, D.J., 2005, Burial of terrestrial organic matter in marine sediments: A re-assessment: Global Biogeochemical Cycles, v. 19, p. 1–7, doi:10.1029/2004GB002368.

Hage, S. et al., 2020, Efficient preservation of young terrestrial organic carbon in sandy turbidity-current deposits: Geology, v. 48, p. 882–887, doi:10.1130/G47320.1.

Hemingway, J.D., Schefuß, E., Spencer, R.G.M., Dinga, B.J., Eglinton, T.I., McIntyre, C., and Galy, V. V., 2017, Hydrologic controls on seasonal and inter-annual variability of Congo River particulate organic matter source and reservoir age: Chemical Geology, v. 466, p. 454–465, doi:10.1016/j.chemgeo.2017.06.034.

Kominz, M.A., Patterson, K., and Odette, D., 2011, Lithology dependence of porosity in slope and deep marine sediments: Journal of Sedimentary Research, v. 81, p. 730–742, doi:10.2110/jsr.2011.60.

Leithold, E.L., Blair, N.E., and Wegmann, K.W., 2016, Source-to-sink sedimentary systems and global carbon burial: A river runs through it: Earth-Science Reviews, v. 153, p. 30–42, doi:10.1016/j.earscirev.2015.10.011.

Reimer, P.J., Brown, T.A., and Reimer, Ron, W., 2004, Discussion: Reporting and Calibration of Post-Bomb 14 C Data: Radiocarbon, v. 46, p. 1299–1304, doi:10.1017/S0033822200033154.

Savoye, B., Babonneau, N., Dennielou, B., and Bez, M., 2009, Geological overview of the Angola-Congo margin, the Congo deep-sea fan and its submarine valleys: Deep-Sea Research Part II: Topical Studies in Oceanography, v. 56, p. 2169–2182, doi:10.1016/j.dsr2.2009.04.001.

Talling, P.J. et al., 2022, Longest sediment flows yet measured show how major rivers connect efficiently to deep sea: Nature Communications, v. 13, p. 1–15, doi:10.1038/s41467-022-31689-3.

Torn, M.S., Swanston, C.W., Castanha, C., and Trumbore, S.E., 2009, Storage and Turnover of Organic Matter in Soil, *in* Biophysico-Chemical Processes Involving Natural Nonliving Organic Matter in Environmental Systems, Hoboken, NJ, USA, John Wiley & Sons, Inc., p. 219–272, doi:10.1002/9780470494950.ch6.

Wacker, L., Christl, M., and Synal, H.A., 2010, Bats: A new tool for AMS data reduction: Nuclear Instruments and Methods in Physics Research, Section B: Beam Interactions with Materials and Atoms, v. 268, p. 976–979, doi:10.1016/j.nimb.2009.10.078.

Fig S1. Timing and runout distance of turbidity current flows recorded by Ocean Bottom Seismometers (OBSs) and Acoustic Doppler Current Profilers in the Congo Canyon-Channel between October 2019 and April 2020.

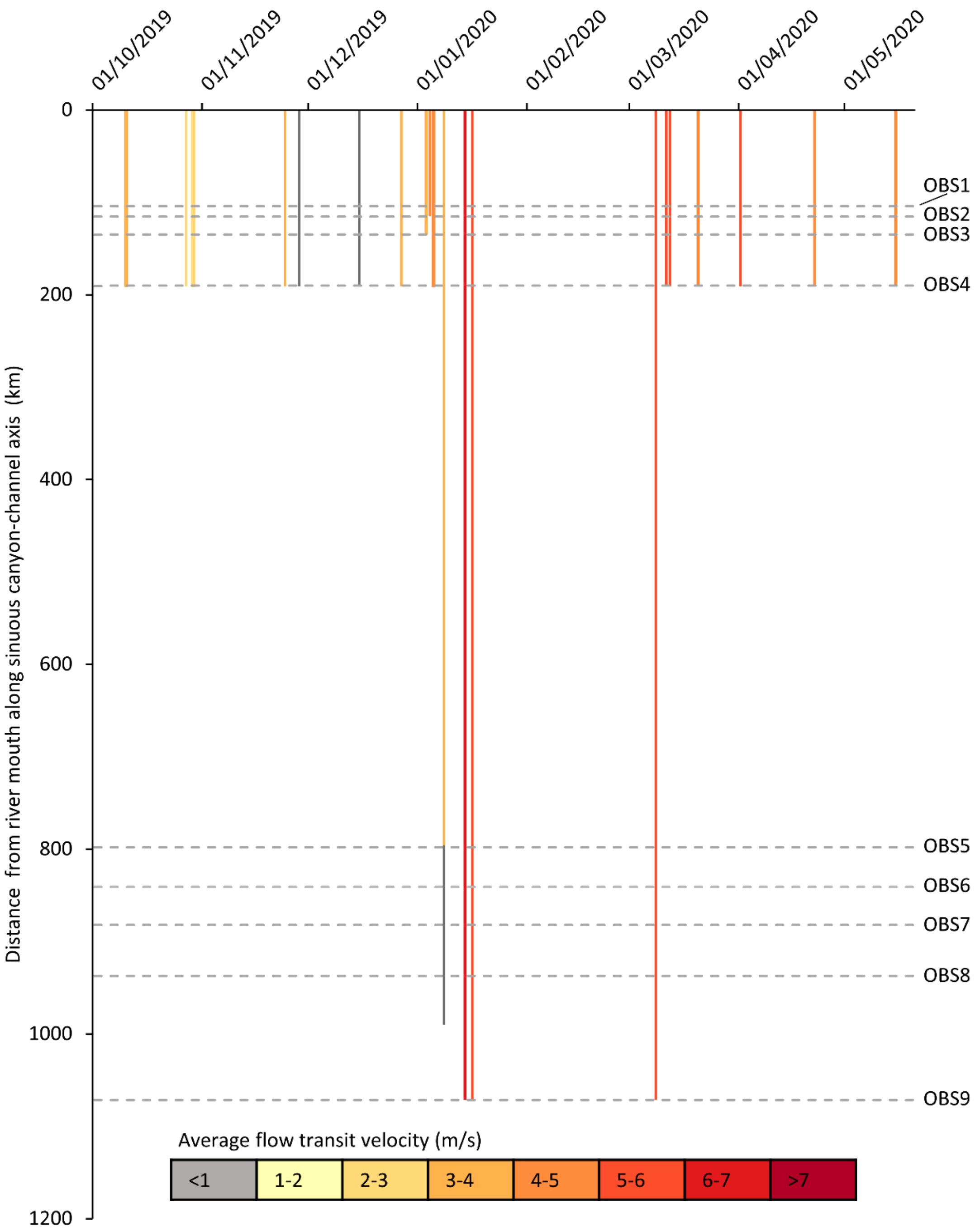

Supplementary Table 1. Length of each facies type in metres in each core

	Length of facies (m)				
Core	Clay	Silt	Muddy sand	Vegetation-rich muddy sand	Sand
1	0	0	0	0	1.50
2	1.37	0.05	1.24	0.00	0.10
3	0.50	0.51	1.04	1.06	1.03
4	5.03	0.60	0.42	0.03	1.38
5	3.45	0.65	1.45	0.33	0.57
6	1.38	4.77	2.71	0.10	0.19
7	5.92	1.74	0.06	0.00	0.00
Total length (m)	**6.93**	**17.65**	**3.28**	**8.33**	**1.52**
Proportion (%)	18.38	46.81	8.69	22.09	4.04

Note: Core 1 was discounted from the calculations as sediment recovery was compromised by bent barrel.

Supplementary Table 2. Average porosity values of the different facies in the Congo Canyon sediment cores

Core	Average porosity per facies per core (%)				
	Clay	Silt	Muddy sand	Vegetation-rich muddy sand	Sand
2	0.80	0.74	0.69		0.64
3	0.76	0.77	0.70	0.80	0.58
4	0.74	0.75	0.64	0.73	0.46
5	0.74	0.65	0.62	0.78	0.68
6	0.77	0.72	0.60	0.71	0.49
7	0.82	0.79	0.78	/	/
Average Porosity (%)	**0.77**	**0.74**	**0.67**	**0.76**	**0.57**
Porosity standard deviation (%)	0.03	0.04	0.06	0.04	0.08

Note: Core 1 was discounted as the sediment had been remobilised.

Supplementary Table 3. Values Needed to Calculate Mass of Sediment and Organic Carbon Eroded in the Congo Canyon Between October 2019 and October 2020

	Facies				
	Clay	Silt	Muddy sand	Vegetation-rich muddy sand	Sand
Facies proportion (%; Table S1)	18.38	46.81	8.69	22.09	4.04
Average facies porosity (%, Table S2)	0.77	0.74	0.67	0.76	0.57
Standard deviation of facies porosity (%, Table S2)	0.03	0.04	0.06	0.04	0.08
Facies density (kg/m^3)	598	676	858	624	1118
Facies density error (kg/m^3)	77	116	156	95	219
Sediment eroded (Mt)	**89**	**48**	**50**	**8**	**31**
Sediment eroded error (Mt)	**12**	**8**	**9**	**1**	**6**
Average facies TOC (%, Table S4)	3.51	2.60	1.81	8.24	0.49
Standard deviation facies TOC (%)	0.60	0.99	1.74	2.24	0.26
Average facies δ13C (‰,Table S4)	-26.72	-26.97	-27.21	-27.32	-27.36
Average facies Fm (Table S4)	0.9446	0.9526	0.9121	0.9881	0.7784
TOC eroded (Mt)	**3.13**	**1.24**	**0.91**	**0.66**	**0.15**
TOC eroded error (Mt)	**0.87**	**0.60**	**0.88**	**0.25**	**0.09**

Supplementary Table 4: Facies Description and Geochemical Data

	Facies description	Average Total Organic Carbon (TOC) and [range] (%)	Average Carbon-Stable Isotope (δ13C) and [range] (‰)	Average Fraction Modern (Fm) and [range]
Clay	Homogeneous or bioturbated clay. Black organic matter particles visible.	**3.51** [5.46 — 2.39]	**-26.72** [-27.30 — -26.29, anomalous value = -23.83]	**0.9446** [0.8484 — 0.9945]
Silt	Homogeneous or bioturbated silty mud. Occasional normal grading to clay or laminated. Often high number of black organic carbon specks.	**2.60** [5.22 — 1.61]	**-26.97** [-27.71—-26.63]	**0.9526** [0.9152 — 0.9814]
Muddy sand	Mixed sand-mud with fine- to medium-grained sand. Occasional floating mud, sand or vegetation-rich muddy sand clasts. Ungraded or normally graded. Organic specks often visible.	**1.81** [0.25 — 6.23]	**-27.21** [-28.45 — -26.38]	**0.9121** [0.8051 — 1.0448]
Vegetation-rich muddy sand	Muddy-sand matrix (fine-grained sand) dominated by mm- to cm-sized black plant debris which can be densely packed.	**8.24** [4.57— 11.32]	**-27.32** [-27.80 — -22.16, anomalous value = -22.16]	**0.9881** [0.9528 — 1.0184, anomalous value = 0.7037]
Sand	Massive, clean fine- to medium-grained sand. occasional floating mud and muddy sand clasts. Often ungraded, occasionally normally graded.	**0.49** [0.15 — 0.88]	**-27.36** [-28.19 — -26.96]	**0.7784** [0.6758 —0.8639]

Supplementary Table 5. Organic carbon geochemistry and grain size on all samples for this study.

ETH number	Sample code	Core depth (m)	Facies	$F^{14}C$ (mean)	$F^{14}C$ uncertainty (%)	Age (y)	Age uncertainty (y)	D_{10} (µm)	D_{50} (µm)	D_{90} (µm)	δ13C (‰)	TOC (%)
	PC04-1-6	0.06	Clay					0.7	5.6	30.4	-26.64	2.98
	PC04-1-90	0.90	Clay					0.7	5.8	29.8	-26.73	2.66
120320.1.1	PC04-2-2	1.21	Silt	0.9699	0.82	245	66	1.2	20.1	98.4		
120321.1.1	PC04-2-23	1.42	Silt	0.9814	0.86	151	69	1.8	48.9	111.9		
120322.1.1	PC04-2-85	2.04	Clay	0.9401	0.82	496	66	1.0	14.2	73.7	-26.58	3.34
120338.1.1	PC04-3-35	3.01	Clay	0.9257	0.86	620	69	0.9	11.4	77.7	-26.59	4.03
120339.1.1	PC04-4-70	4.00	Clay	0.9945	0.84	44	68	1.1	13.9	69.5	-26.39	3.99
120340.1.1	PC04-4-90	4.20	Clay	0.9594	0.86	333	69	1.2	11.8	65.2	-26.33	5.46
120341.1.1	PC04-5-15	5.97	Clay	0.9533	0.85	384	68	0.8	7.9	49.3		3.79
120342.1.1	PC04-5-115	4.97	Clay	0.9520	0.84	395	67	0.9	10.6	55.2		3.93
120343.1.1	PC04-6-60	7.59	Clay	0.9770	0.84	187	68	1.1	11.1	46.9		
120344.1.1	PC04-6-130	6.89	Clay	0.9161	0.85	704	68	1.1	13.5	61.7		
120927.1.1	PC07-1-10	0.10	Sand	0.7377	0.95	2,443	77	72.0	129.6	211.9		
	PC07-1-50	0.50	MS					3.3	168.6	500.3	-27.50	0.63
120986.1.1	PC07-1-95	0.95	MS	0.8455	0.89	1,348	71	7.1	127.9	375.8	-27.42	0.82
120990.1.1	PC07-2-5	1.51	Clay	0.9631	0.84	302	68	0.8	6.0	29.4	-27.30	3.92
120984.1.1	PC07-2-55	2.01	Silt	0.9478	0.85	431	68	1.5	45.7	187.0	-27.12	2.61
120991.1.1	PC07-3-35	2.39	Silt	0.9806	0.85	158	69	1.2	34.4	148.1	-27.32	2.14
120931.1.1	PC07-3-90	2.94	MS	0.9562	0.81	360	65	3.1	86.5	187.9		2.39
120939.1.1	PC07-3-110	3.14	VRMS	0.9973	0.81	22	65	9.5	100.4	190.2	-27.52	7.90
120930.1.1	PC07-3-136	3.40	MS	1.0448	0.81	0	65	5.0	102.9	231.5	-26.38	6.23
120935.1.1	PC07-4-60	4.11	Clay	0.9346	0.80	543	65	0.8	7.7	37.3		
120992.1.1	PC07-4-110	4.61	MS	0.9429	0.85	472	68	2.5	79.2	290.3	-27.21	1.93
120988.1.1	PC07-5-5	5.03	Clay	0.9537	0.86	381	69	0.9	11.3	77.8	-27.00	3.19
120938.1.1	PC07-5-70	5.68	MS	0.8051	0.88	1,741	71	50.7	205.6	452.7	-28.45	0.25

120940.1.1	PC07-5-122	6.20	Clay	0.9436	0.80	466	64	0.9	6.2	26.9	-27.13	3.65
120285.1.1	PC08-1-1	0.01	VRMS	0.9721	0.83	227	67	5.4	89.1	187.6	-26.98	6.46
120286.1.1	PC08-1-90	0.90	Clay	0.9932	0.84	55	67	1.1	8.3	45.1	-26.67	3.68
120287.1.1	PC08-2-25	1.72	Clay	0.9499	0.85	413	68	0.9	9.7	58.1	-27.07	2.39
120288.1.1	PC08-2-110	2.57	Silt	0.9721	0.84	227	67	1.2	20.6	91.4	-26.78	2.27
120289.1.1	PC08-3-8	2.98	Clay	0.9605	0.84	324	68	0.9	10.9	65.3		3.35
120290.1.1	PC08-3-11	3.01	Sand	0.7509	0.99	2,301	79	36.7	122.6	224.7	-26.91	
120291.1.1	PC08-3-70	3.60	Clay	0.9607	0.82	322	66	1.0	6.6	29.3	-26.59	3.49
120292.1.1	PC08-4-31	3.92	Silt	0.9152	0.86	712	69	1.4	37.3	283.2	-26.74	1.75
120293.1.1	PC08-4-80	4.41	Clay	0.9720	0.84	229	68	0.9	8.2	49.0	-26.76	3.93
120294.1.1	PC08-4-130	4.91	Clay	0.9429	0.84	472	67	0.9	6.7	29.9	-26.85	3.25
120295.1.1	PC08-5-34	5.42	MS	0.8394	0.88	1,406	71	3.0	88.4	206.7	-26.88	1.08
120296.1.1	PC08-5-85	5.93	Sand					91.4	188.4	322.4	-27.19	
120297.1.1	PC08-5-135	6.43	Sand	0.6758	0.98	3,148	79	106.1	279.6	505.9	-27.30	
120298.1.1	PC08-6-50	6.99	Sand	0.7811	0.93	1,985	75	95.0	231.5	465.8	-27.31	0.15
120299.1.1	PC08-6-100	7.49	Clay	0.8737	0.84	1,085	67	0.9	9.0	59.3	-26.52	2.66
120284.1.1	PC08-6-142	7.91	MS	0.8863	0.85	970	68	4.0	127.8	308.5	-26.91	1.20
120936.1.1	PC12-1-12	0.12	Sand	0.7525	1.07	2,284	86	83.3	196.2	411.5		
120934.1.1	PC12-1-25	0.25	Silt	0.9770	0.81	187	65	1.9	51.3	184.4		
	PC12_1_50	0.50	MS					3.8	87.6	212.8	-27.37	1.48
120932.1.1	PC12-1-70	0.70	MS	0.9857	0.84	116	68	4.7	86.6	332.9	-26.90	6.22
120933.1.1	PC12-1-100	1.00	VRMS	0.9528	0.83	389	67	5.9	86.9	256.0	-27.80	9.95
120989.1.1	PC12-2-40	1.60	Sand	0.8639	0.87	1,176	70	2.5	86.8	203.0	-27.30	0.88
120987.1.1	PC12-2-85	2.05	VRMS	0.9999	0.84	0	68	6.7	90.3	231.2	-27.25	11.32
120985.1.1	PC12-2-130	2.50	Clay	0.8484	0.89	1,320	72				-26.36	3.03
120929.1.1	PC12-3-15	2.82	MS	0.9606	1.10	323	88	2.0	68.2	179.7	-27.45	4.14
120928.1.1	PC12-3-37	3.04	Sand	0.8155	0.88	1,639	70	12.6	127.9	308.5	-26.96	0.49
120937.1.1	PC12-3-50	3.17	Clay	0.8578	0.82	1,232	66	1.1	7.7	37.7	-26.29	3.87
	PC12_3_66	3.33	Sand					68.6	176.9	354.2	-28.01	0.27
	PC12_3_110	3.77	Sand					79.4	202.7	426.7	-27.11	

120345.1.1	PC14-1-2	0.02	Silt	0.9444	0.88	460	70	5.5	60.8	119.3	-27.12	1.61
	PC14-1-50	0.50	Clay					0.7	5.0	19.2	-27.19	3.28
	PC14-1-95	0.95	MS					49.7	105.8	153.3	-27.65	0.38
120925.1.1	PC14-2-11	1.39	Silt	0.9270	0.85	609	68	1.4	23.4	241.6	-27.71	3.36
120926.1.1	PC14-2-14	1.42	Sand	0.8497	0.85	1,309	68	7.1	105.8	281.5	-28.19	0.65
120924.1.1	PC14-2-65	1.93	MS	0.8834	0.84	996	68	4.6	64.8	120.7	-26.86	0.96
	PC14-2-120	2.48	Silt					1.9	39.1	130.0	-26.63	5.22
120316.1.1	PC16-1-10	0.10	Sand					94.8	156.4	232.5		
120317.1.1	PC16-1-135	1.35	Sand					114.0	230.8	413.8		
120300.1.1	PC17-1-2	0.02	Clay	0.9455	0.82	450	66	1.2	8.2	41.2	-23.83	3.32
120301.1.1	PC17-1-50	0.50	MS	0.9358	0.84	533	68	2.9	84.8	181.6	-27.19	1.50
120302.1.1	PC17-2-59	1.10	MS	0.9080	0.84	776	68	2.0	71.2	342.1		1.14
120303.1.1	PC17-2-100	1.51	MS	0.9374	0.84	519	67	2.8	101.1	336.2	-27.15	1.43
120304.1.1	PC17-2-140	1.91	MS	0.9450	0.84	454	67	1.9	76.0	275.7		
120305.1.1	PC17-3-45	2.45	Silt	0.9470	0.84	438	67	1.3	26.6	157.7	-26.65	2.56
120306.1.1	PC17-3-87	2.87	Silt	0.9431	0.84	471	68	1.5	42.9	262.5	-26.95	2.20
120307.1.1	PC17-4-50	4.01	MS	0.8484	0.88	1,321	71	6.3	97.5	202.8	-26.94	0.49
120308.1.1	PC17-4-120	4.71	Silt	0.9155	0.84	709	68	1.6	27.0	127.4	-26.71	2.31
120309.1.1	PC17-5-55	5.36	MS	0.9192	0.85	677	68	3.9	67.9	139.6	-27.27	1.44
120310.1.1	PC17-5-58	5.39	Clay	0.9731	0.82	219	66	0.8	8.5	54.1	-26.76	3.10
120311.1.1	PC17-6-50	6.73	MS	0.8692	0.88	1,126	70	6.4	136.4	380.4	-27.16	0.61
120312.1.1	PC17-6-130	7.53	Clay	0.9668	0.83	271	67	0.9	8.8	39.6	-26.64	3.91
120313.1.1	PC17-7-70	8.43	Clay	0.9751	0.85	203	68	0.9	8.0	42.1	-26.81	3.47
120314.1.1	PC17-7-128	9.01	VRMS	1.0184	0.84	0	68	53.9	108.1	164.6	-22.16	4.57
120315.1.1	PC17-7-135	9.08	VRMS	0.7037	0.97	2,822	78	41.2	149.6	278.8	-27.03	9.26

Note: For facies, VRMS = vegetation-rich muddy sand, MS = muddy sand